BNL-34595

CONF-840405--12

BNL--34595

DE84 010890

INTERGRANULAR FAILURES OF ALLOY 600 IN HIGH TEMPERATURE CAUSTIC ENVIRONMENTS

R. Bandy, R. Roberge* and D. van Rooyen

Materials Research Group
Department of Nuclear Energy
Building 703M
Brookhaven National Laboratory
Upton, NY 11973

ABSTRACT

This paper describes the results of our investigation of two commonly observed modes of failure of Alloy 600 in high temperature caustic environment namely, intergranular stress corrosion cracking (IGSCC) and intergranular attack (IGA). Specimens are studied as C-rings under constant deflection, wires with and without any externally applied load, and as straining electrodes. The potential dependence of average crack propagation rate is established in a single test by using several C-rings held at different potentials, by using a modification of the static potential gradient method of Seys and Van Haute. SCC appears to be governed by a film rupture mechanism and its propagation rate is significantly influenced by the electrochemical potential and associated surface film formation. The maximum crack propagation rate for C-rings and constant load specimens is very similar but much smaller than that calculated for a straining electrode at the same potential. IGA occurs over a wide range of potential -- starting from a few tens of millivolts cathodic to the corrosion potential up to the lower end of anodic potentials normally required for SCC. IGA seems to be rather independent of stress and is generally more pronounced in the crevice area under the nuts used in C-rings. Examination of several creviced coupons shows that outside the crevice, enrichment of iron and chromium occurs on the surface as the potential is raised anodically, whereas the Ni:Fe and Ni:Cr ratios remain relatively independent of potential within the crevice. It is believed that a better knowledge of the crevice chemistry and its mass transport characteristics will provide a clue to the origin and extent of IGA.

*Visiting scientist from Institut de recherche d'Hydro-Quebec, Canada.

INTRODUCTION

Intergranular stress corrosion cracking (IGSCC) and intergranular attack (IGA) are the two most common types of failure of Alloy 600 materials in the caustic environment. A combination of SCC and IGA has been observed in Alloy 600 tubing on the hot leg of some operating steam generators in pressurized water reactor nuclear power plants, and sodium hydroxide along with several other chemical species have been implicated for the tube degradations[1-9]. SCC has been observed above and within the tubesheet, whereas IGA is generally noticed within the tubesheet[1,2]. Various factors that influence SCC and IGA include metallurgical conditions of the alloy, concentration of alkaline species, impurity content, temperature and stress[1-9].

In short-term laboratory tests with stressed specimens in caustic environments, both SCC and IGA have been detected. However, one generally observes more extensive SCC and less extensive IGA in these laboratory specimens than in the tubing removed from the field[3]. The mechanisms of intergranular failures of Alloy 600 in high temperature environments are not well understood. It is not clear whether SCC and IGA are two aspects of the same phenomenon or whether they are governed by independent processes. This investigation was aimed at understanding the mechanisms of SCC and IGA of Alloy 600 in high temperature caustic environments, with a special emphasis on the electrochemical aspects of the two processes.

EXPERIMENTAL

Our investigation was conducted using C-ring, constant load and straining electrode specimens. For C-rings, a nuclear grade Alloy 600 tubing, 19.1mm OD and 1.07mm wall thickness, was used. Its composition is shown in Table 1. An Alloy 600 wire of 0.51mm diameter but unknown composition was used for the constant load and straining electrode tests.

The materials were mainly used in their mill annealed (MA) conditions. A few C-ring specimens were tested in a solution annealed (SA) and solution annealed plus sensitized (SAS) condition. SA samples were heat treated at 1050°C for 10 min. and rapidly air cooled. SAS samples were heated at 1100°C for 10 min. and water quenched before sensitization at 621°C for 18 h. Heating was in sealed tubes with an inert atmosphere to prevent oxidation. The C-rings were stressed on their OD in the usual way[10]. The mill annealed material was stressed at a strain corresponding to 150% of yield strength. The same deformation as for the MA material was applied on the SA and SAS C-rings. Since the yield strength of the SA and SAS materials was lower than that of the MA material, the applied tensile stress at the apex of the C-rings was less for the heat treated materials than for the MA one.

Before testing, the specimens were degreased in acetone, then in methanol, and allowed to dry in air. When appropriate, some specimens were examined for localized attack under the microscope after removing ultrasonically any loosely attached surface oxides or deposits.

The solutions were prepared from distilled demineralized water of conductance < 0.5 μS. Reagent grade sodium hydroxide (NaOH) pellets were used to prepare the solutions. In some cases, controlled amounts of sodium carbonate and sodium sulfate were added as impurities. All tests were conducted in the 300-315°C range for generally about 10 to 12 days.

The static potential band method[11] used to control the potentials of the specimen(s) consisted, in the case of the C-rings, of passing a large current from a power supply through a string of samples separated from one another by a known electrical resistor while holding one of them at a fixed potential with a potentiostat. An iR drop was thus established between each sample of the series causing each one to attain a different electrochemical potential. In the wire experiment, the wire itself acted both as the specimen and the electrical resistor allowing a continuous iR drop to occur along its length. Alloy 600 leads were connected to various C-rings or points on the wire to monitor their potentials. In some tests there was a drift in the potentials, and when a potential shift of about 15 mV had occurred on any of the samples, the experiment was ended. The reference electrode was made of nickel and the nickel autoclave body acted as the counter electrode[12]. Before raising the temperature, the autoclave was deaerated by pressurizing to 3.45 MPa (500 psi) with nitrogen followed by a slow depressurization , the procedure being repeated five times. A 1.38 MPa overpressure of 5% hydrogen -95% nitrogen was then added. When a stable corrosion potential was established at the testing temperature, the potentiostat and power supply were switched on.

In the constant load test, the 0.51mm diameter wire was loaded to a nominal stress of 221 MPa i.e., about 65% of the yield strength. A continuous potential gradient along the wire was established using the Seys and Van Haute technique described before.

The straining electrode test was conducted under potentiostatic control following procedures described previously[13,14]. Prior to straining, the desired potential was applied to the specimen and the current was allowed to reach a steady value. The specimen was then rapidly strained at a rate of about 1% per second into the plastic region. The current transient thus caused was recorded, and used to calculate the crack propagation rate.

Potentiodynamic polarization was conducted using a PAR Model 173 potentiostat and HP Model 7047 X-Y recorder. An ELSCINT Model ABA-26 automatic Baseline Advance was used to obtain the desired scan rate. Potential was recorded vs. the nickel reference electrode.

In another set of experiments, Alloy 600 coupons (12.5mm x 25mm) were exposed to the same environment and potentials as the C-rings. The coupons were polished with diamond paste to 1 μm finish. Each coupon had a 4mm diameter central hole. Using Alloy 600 bolt and square nuts, a crevice of about 8mm x 8mm was created in the centre of the coupon. After withdrawal from the environment, the surfaces inside the crevice and outside were examined under optical and scanning electron microscope and analyzed by energy dispersive X-rays (EDX).

RESULTS

The microstructure of the tubing material used for C-ring tests is shown in Figs. 1(a) and (b) after a 8:1 H_2O:H_3PO_4 electrolytic etch and a 5% Nital electrolytic etch respectively.

C-Ring Tests

The SCC test results with multiple C-rings using the modified Seys and Van Haute technique are shown in Fig. 2. The tests were run in 10% NaOH+ 0.1% Na_2CO_3 at 300°C. The crack propagation rate shown is the average value based on the total testing time and the maximum crack depth. The specimens were tested under mill annealed (MA), solution annealed (SA), and "sensitized" (SAS) conditions, as shown on the diagram. All the MA C-rings held between 100 mV and 220 mV underwent SCC, with a maximum crack propagation rate at +177 mV. Similar potential dependence of SCC was observed by various previous investigators[15-17]. Some of the SA and SAS specimens also cracked in the potential zone studied, but generally with a marked difference in the maximum crack depth.

IGA was observed in this environment on the MA C-rings over a wide range of potential - from about -84 mV up to about 60 mV. Some of these samples showing IGA were exposed in the environment in two successive test runs for a total of 343 hours. Fig. 3(a) shows a typical IGA attack in its early stage on a MA C-ring held between 12 and 20 mV for 343 hours. The maximum depth of IGA on these samples varied from 50 to 140 μm and no difference was observed in its extent against potential within the range mentioned above. Unlike SCC, shown typically in Fig. 3(b), IGA spread laterally on the surface and penetrated only a few grains. In some samples suffering SCC, there were areas where both SCC and some shallow IGA were observed. The SA C-rings also showed IGA between -50 to +80 mV in a 10 day test in the above environment, although the attack was generally shallower than that in the MA samples.

Tests in 10% NaOH + 1% Na_2CO_3 solution gave a potential dependence of SCC very similar to that in the 10% NaOH + 0.1% Na_2CO_3 solution except that in the previous environment SCC was observed at a more active potential than in the latter environment, e.g., at about +40 mV.

Tests were also run in 10% NaOH with 0.1% and 1% Na_2SO_4 addition. The potential dependence of crack propagation rates were very similar to that in 10% NaOH with carbonate contaminations. The solution with 1% Na_2SO_4 addition was again a little more aggressive than the one with 0.1% Na_2SO_4 in that SCC occurred at a more active potential ($\sim$40 mV) in the previous environment. Shallow IGA was noticed in the sulfate contaminated solutions at potentials very similar to those observed in the carbonate contaminated ones.

In a 1% NaOH + 1% Na_2CO_3 environment, MA samples were maintained between -90 and 220 mV for 240 hours. The only sample that suffered SCC was at +170 mV, giving an average propagation rate of 0.2 μm/h. No IGA was noticed in any of these specimens.

Constant Load Tests

The first constant load test, reported was carried out at 315°C in 1% NaOH solution contaminated with 0.01% Na_2CO_3. With 221 MPa (32000 psi) applied stress the 0.51mm diameter MA wire did not fail in the 10 day exposure. After resin mounting the piece of wire exposed to the solution, polishing to 1 μm and etching with 8:1 phosphoric acid etchant, the metallographic observation revealed incipient intergranular corrosion. It started near -40 mV and ran to about +45 mV, with apparently a maximum in the attack around +20 mV. On each side of the attacked region, the localized corrosion disappeared. The wire polarized to about 200 mV showed no SCC.

The second experiment, also in a MA condition, tested the effect of a 10% NaOH solution contaminated with 0.1% Na_2CO_3. The wire broke in less than 3 days by intergranular SCC at about 210 mV. On each side of the fracture surface deep cracks had already initiated and oxide grooving was observed from about 160 mV to 220 mV (Fig. 4).

Test on Unstressed Wire

This test with the MA wire without any applied stress was carried out at 300°C in 10% NaOH contaminated with 1% Na_2CO_3. It lasted 10 days. Potentials between -130 mV to 350 mV were covered. The cathodic part of the wire was unfortunately destroyed during polishing.

However, the metallographic examination from about 30 mV anodic to the corrosion potential revealed different areas of continuous grooves and of scattered IGA. The first area was generally characterized by large grooves making their way into the grain boundaries and covered the entire length through about 125 mV and contained some IGA. The surface between about 125 mV to 165 mV was clean, while from there to 270 mV some scattered grooves reappeared. Beyond 270 mV no kind of grain boundary grooving was observed.

Straining Electrode Test

This test, aimed at obtaining the maximum crack propagation rate (CPR) was performed in 10% NaOH + 0.1% Na_2CO_3 in the potential range of 150 to 250 mV. The steady state and transient current after load pulsing were noted at each potential. The current measured during straining, i_y, is given by [14].

$$i_y = (i_s \times A_s) + (i_b \times A_b) \qquad (1)$$

where,

i_s = current density on the filmed metal

A_s = fraction of specimen area covered by the film

i_b = current density on the bare metal

A_b = fraction of specimen with bare metal

It is assumed that i_s remains constant during straining and the transient current comes from the dissolution of the newly exposed bare metal where the film breaks. The amount of fresh surface produced due to straining is:[18]

$$\% \text{ Bare surface} = 100 \left[1 - \frac{L_o}{L}\right]^{1/2} \quad (2)$$

where L_o is the initial length and L is the length at any time during straining. For small linear strains, equation (2) reduces to:[14]

$$\% \text{ Bare surface} \simeq 1/2(\% \text{ strain}) \quad (3)$$

Equation (2) was derived on the assumption that the surface film is adherent but brittle compared to the metal substrate[18].

The following typical current density values were obtained in our test:

i_s = 1.0 mA/cm^2

i_b = 20.9 mA/cm^2 at $\sim$ 200 mV.

The maximum CPR, V_m, is related to the maximum i_b value through the equation:[14]

$$V_m = \frac{i_b E}{Fd} \quad (4)$$

where E, is the mean equivalent weight for the metal, d its density and F the Faraday Constant. Using an E of 29 g/eq, and d of 8.5 g/cm^3 for Alloy 600[13], one obtains the maximum CPR, V_m = 26.6 μm/h.

Polarization Curve

Fig. 5 shows the potentiodynamic polarization curve of Alloy 600 in 10% NaOH + 1% Na_2CO_3 at 300°C at a scan rate of 20 mV/min. The polarization curve in 10% NaOH + 1% Na_2SO_4 at 300°C was essentially similar to that in Fig. 5. In 10% NaOH solution, however, although the active peak current and the potential for active to passive transition were very similar to the curve shown in Fig. 5, the passive current density was about 40% smaller than that in Fig. 5. Polarization scans at a slower rate of 1 mv/min. and a faster rate of 500 mV/min. were also obtained. Increasing scan rate increased the value of the anodic peak current and the potential for active-passive transition. For example, in 10% NaOH + 1% Na_2SO_4 at 300°C, at 500 mV/min, the above two values were 37.8 mA/cm^2 and 190 mV respectively, compared to about 12 mA/cm^2 and 120 mV at 20 mV/min. The regions of SCC and IGA as commonly observed in our tests, are delineated in Fig. 5.

Surface Attack on Creviced Coupons

Fig. 6 (a) - (b) show the nature of surface attack on an Alloy 600 coupon in 10% NaOH + 1% Na_2SO_4 outside and inside the crevice after a 10 day exposure. The specimen was held at a potential in the range of -40 to -55 mV. The EDX analysis of the matrix region or the particles in Fig. 6(a) gave only nickel spectra, presumably from cathodic deposition of nickel in preference to iron and chromium. The area under the crevice appears very different from that outside the crevice and the spectra consist of nickel, iron and chromium. Table 2 summarizes the Ni:Fe and Ni:Cr for various coupons inside and outside the crevice in various samples examined in this environment. The flake mentioned in Table 2 refers to the small flaky deposit in Fig. 6(b). Fig. 6(c)-(d) illustrate the surfaces outside and inside the crevice of the coupon that was held at 0 mV. The spectra for various regions, shown in Table 2, show that some particles outside the crevice were highly enriched in chromium, whereas others were pure nickel. Inside the crevice, some particles were also enriched in chromium. Fig. 6(e)-(f) represent the areas outside and inside the crevice for a coupon at 25 to 45 mV. The area outside the crevice is generally etched, but some areas were completely covered with a dark film. EDX indication from the oxide and outside the oxide were very similar, presumably because the film was very thin. The area inside the crevice was filled with a dark film with regions of relatively thicker deposits, giving spectra different from those in the matrix. The nature of attack on the specimen held at 60 to 80 mV was very similar to that at 25/45 mV with patches of dark oxide on a generally etched surface outside the crevice, and dark deposits inside the crevice with some scattered particles. The surface of the coupon held at 150 mV was mostly covered with a black film with some isolated bare areas as shown in the optical micrograph in Fig. 6(g) showing the filmed and the stripped areas. The spectra from the film shows considerable enrichment in iron and chromium (Table 2) compared to that in the stripped area which probably resembles the Alloy 600 substrate. However, the fact that the oxide composition is so different from the material underneath implies that it is thicker than that observed at lower potentials. Fig. 6(h) shows details of attack in the stripped area in Fig. 6(g), revealing considerable grain boundary grooving. The area inside the crevice in this sample showed a range of attack, as shown typically in Fig. 6(i) and (j) for two different areas within the crevice.

DISCUSSION

The SCC testing with multiple C-rings using the modified Seys and Van Haute technique proved to be a very successful method leading to considerable saving in testing time and eliminated variations that can occur between individual tests. Our data in Fig. 2 are in excellent agreement with those of earlier investigators[15-17], thus giving necessary support for the validity of the method. The technique has recently been used successfully to study SCC at room temperature[19].

Fig. 2 shows that the CPR of the MA material is much higher than that of the SA or the SAS materials. However, because of the heat treatment, the SA and SAS materials have much lower yield strength, and since all our C-rings were given the same amount of deflection, the stress level reached by the SA and SAS C-rings were lower than that of the MA C-rings. Therefore, it is not clear whether this factor is responsible for an apparent improvement in SCC performance or whether the heat treatments actually improved SCC resistance. In the literature, there is ample evidence that sensitizing heat treatments generally improve the caustic SCC resistance of Alloy 600[15,17]. However, these tests were conducted with C-rings or other constant deflection type specimens and it is not clear whether the heat treatment improves the SCC resistance by merely improving the initiation behavior. Tests with precracked wedge-opening-load specimens in 50% NaOH showed that the SAS specimens of Alloy 600 actually registered greater crack growth than SA or MA type specimens[20].

Addition of 1% Na_2CO_3 or 1% Na_2SO_4 to 10% NaOH appears to cause SCC at a somewhat more active potential than in 10% NaOH solution. The maximum CPR was not significantly affected by the above additions of carbonate and sulfate to the 10% NaOH solution and no appreciable distinction between the carbonate and sulfate effects at this level of caustic could be noticed.

The maximum average crack propagation rate observed with C-rings was about 6 to 7 μm/h and that with the constant load test on the wire was about 8 μm/h. These values are based on the total testing time which includes initiation. Therefore, the net CPR would be even much higher. With fatigue precracked type WOL or DCB specimens, Berge and Donati[21] obtained a stage II crack propagation rate of somewhat greater than 6 μm/h in 10% NaOH at 350°C. These tests were, however, without any potential control and it is likely that the maximum growth rate in their system would be much higher and possibly closer to the 26.6 μm/h value calculated by us in our straining electrode tests. Thus, there is a need for further tests with precracked specimens under potential control to confirm this.

The onset of rapid SCC generally coincides with the potential corresponding to the active-passive transition, and at potentials where the passivity is well established (> 300 mV), crack growth rate falls sharply. This suggests a film rupture type model for the SCC process. Thus, cracking proceeds due to the rupture of the film caused by transient creep followed by anodic dissolution along the grain boundary and subsequent repassivation. The grain boundary grooving in coupons, held in the potential region of 150 to 200 mV, Fig. 6(h), clearly demonstrates that grain boundaries are preferred sites for active corrosion process, thus accounting for the intergranular cracking. Grain boundaries could influence SCC in a number of ways. First, strain is likely to be greater near the grain boundary which may also be the site of numerous dislocation pile-ups. Second, the composition of the grain boundary may differ from the bulk composition. Thus, in a narrow region at or adjacent to the grain boundary, an anodic area may be postulated, especially if there is large misorientation between abutting grains or segregation of a particular harmful species at the boundary.

The slowest scan rate used in obtaining our polarization curve was 1 mV/min which gave a potential for active-passive transition of about 100 mV and with higher scan rate this potential moved in the noble direction. It is conceivable, therefore, that at very slow scan rate or under steady state conditions, this potential would be active to 100 mV. This is in agreement with our results on coupons where a partially filmed covered surface is observed at a relatively active potential (Fig. 6(e)). In our tests with C-rings under potential control, no SCC was observed at 0 mV in 10-12 days. However, there are numerous reports in the literature of SCC of open circuit C-rings. This apparent contradiction can be resolved if one bears in mind that these open circuit tests are usually long term tests where the corrosion potential of the specimen gradually drifts anodically and eventually reaches a potential conducive to film formation, leading to SCC.

In the potential region where the coupons are partially covered with a film, the anodic potential limit of IGA overlaps the lower limit of the SCC region. This observation may allow a tentative assumption that stress is possibly not an important factor in the initiation of IGA in that range of potential. Indeed, in this overlapping region, as soon as a reasonable stess is applied, it probably modifies the IGA mechanism into a pure SCC mechanism. However, in the region where no SCC normally initiates (-80 mV to +20 mV) the effect of stress on the rate of IGA may be a significant component although this must be confirmed by more work. So far, the results obtained from the C-ring experiments showed that IGA was produced on the samples held between about -80 mV to 80 mV. Also, the constant load test in 1% NaOH + 0.01% Na_2CO_3 showed more or less regular, shallow attack between about -40 mV to +45 mV.

The two preceding factors of electrochemical potential and stress component may explain the SCC "fingers" sometimes emananting from the base of IGA on the outside diameter of the C-ring. In one case any ingress of oxidizing species (oxygen, copper) inside the IGA network might increase the potential, thus modifying to a SCC mechansim the previous form of corrosion. In a second situation when IGA develops in a relatively oxidizing environment without enough stress to generate cracking, the IGA process may continue until a stress is somehow reached or applied to the affected areas.

In all our C-ring tests, the most pronounced IGA generally occurred under the nuts and often on the compressive side. This observation coupled with the fact that in steam generator IGA generally occurs within the tubesheet area leads us to believe that this type of attack is perhaps governed by a somewhat different electrochemical process than SCC. Inside the crevice there is an IR drop due to the resistive path of the crevice and also limited mass transport which will cause the dissolved ions to often exceed their solubility limit, leading to precipitation, salt film formation or crystal growth. Even our limited attempt with creviced coupons shows that the nature of attack inside the crevice is very different from that outside. Also, EDX analyses show (Table 2) that while outside the crevice there is considerable enrichment of

iron and chromium on the surface as the potential is raised, the Ni:Fe and Ni:Cr ratios remain relatively independent of potential within the crevice (on the matrix of the crevice and not the deposits), thus implying that a mass transport-limited process is operative inside the crevice. Therefore, a thorough knowledge of the crevice chemistry, especially in as complex an environment as that in the steam generator, is required before one can reliably predict the nature and extent of IGA.

CONCLUSIONS

1. The static potential gradient method appears to be a valuable technique for high temperature autoclave testing in aggressive environments

2. Both potential areas of IGA and SCC are defined. Starting cathodic to the corrosion potential, IGA runs through anodic potentials to the lower end of the region of SCC.

3. SCC in caustic seems to be governed by a film rupture mechanism. The rate of SCC is significantly influenced by the electrochemical potential and associated surface film formation.

4. The calculated maximum CPR determined by the straining electrode is much higher than that of C-ring or the constant load specimens at the same potential.

5. In C-ring tests, the most pronounced IGA generally occurs under the nuts, i.e., in the crevice. A more thorough knowledge of the crevice chemistry and its mass transport characteristics is required in order to predict reliably the nature and extent of IGA.

ACKNOWLEDGEMENTS

This work was supported by the Electric Power Research Institute. Discussion with J. P. N. Paine and A. R. McIlree are gratefully acknowledged. Thanks are due to C. Schnepf, T. Roberts and J. Svandrlik for technical assistance.

REFERENCES

1. Green, S.J. and Paine, J.P.N., Nuclear Technology, 55, 10(1981).

2. Pement, F.W., Environmental Degradation of Engineering Materials in Aggressive Environments, Proc. 2nd. Int. Conf. on Env. Degrad. of Eng. Materials, Virginia Polytech. Inst., Blacksburg, Va., Sept. 21-23, 1981, p. 329.

3. Airey, G.P, and Pement, F.W., Corrosion, 39, 46 (1983).

4. Wilson, I.L.W., Pement, F.W., Aspden, R.G. and Begley, R.T., Nuclear Technology, 31, 70 (1976).

5. Wilson, I.L.W, and Aspden, R.G., Corrosion, 32, 193 (1976).

6. Pement, F.W., Wilson, I.L.W. and Aspden, R.G., Materials Performance, 19, 43 (1980).

7. Paine, J.P.N., NACE Corrosion/82, Paper No. 204(1982).

8. Theus, G.J., Corrosion, 33, 20 (1977).

9. Pathania, R.S., Corrosion, 34, 149 (1978).

10. Berge, Ph., Donati, J.R., Prieux, B. and Villard, D., Corrosion, 33, 425(1977).

11. Seys, A.A. and Van Haute, A.A., Corrosion, 29, 329 (1973).

12. Cels, J.R., Corrosion, 34, 198(1978).

13. Park, Y.S. Galvele, J.R., Agrawal, A.K. and Staehle, R.W., Corrosion, 34, 413 (1978).

14. Maier, I. and Galvele, J.R., Corrosion, 36, 60(1980).

15. Theus, G.J. and Cels, J.R. in Stress Corrosion Cracking - The Slow Strain - Rate Technique, ASTM STP 665, C.M. Ugiansky and J. H. Payer, Eds., ASTM, pp. 81-96 (1979).

16. Pessall, N., Corrosion Science, 20, 225 (1980).

17. Pessall, N., Airey, G. P. and Lingenfelter, B. P., Corrosion, 35, 100(1979).

18. Bubar, S.F. and Vermilyea, D. A., J. Electrochem. Soc., 113, 892 (1966).

19. Bandy, R. and van Rooyen, D. Corrosion in Press.

20. Sedriks, A. J., Floreen, S. and McIlree, A.R., Corrosion, 32, 157(1976).

21. Berge, Ph., and Donati, J. R., Nuclear Technology, 55, 88 (1981).

TABLE 1

Chemical Analysis of Alloy 600 Tubing Used in C-rings (W%)

C	Mn	Fe	S	Si	Cu	Ni	Cr	Al	Ti	Co	P	B
0.02	0.23	9.40	0.001	0.14	0.30	74.27	15.64	0.24	0.31	0.04	0.011	0.005

TABLE 2

EDX Analyses of Creviced Coupons Exposed to 10% NaOH + 1% Na_2SO_4 Solution at 315°C for 240 Hours

Potential of Samples	Ni:Fe Ni:Cr	Outside Crevice				Inside Crevice			
		Matrix	Oxide	Particle type 1	2	Matrix	Deposits on Matrix	Particle	Flake
-40 to -55 mV		Ni	-	Ni	-	4.58 2.25	-	-	5.05 1.93
0 mV		13.74 7.35	-	2.63 0.19	Ni	4.77 2.24	-	3.31 1.30	-
25 to 45 mV		4.82 2.22	4.81 2.23	-	-	5.79 2.60	7.87 3.93	-	-
60 to 80 mV		5.03 2.46	4.83 2.13	-	-	-	-	1.89 1.23	-
150 mV		6.20* 2.78*	0.64 0.44	-	-	-	-	-	-

Note: *refers to area where oxide film was stripped.

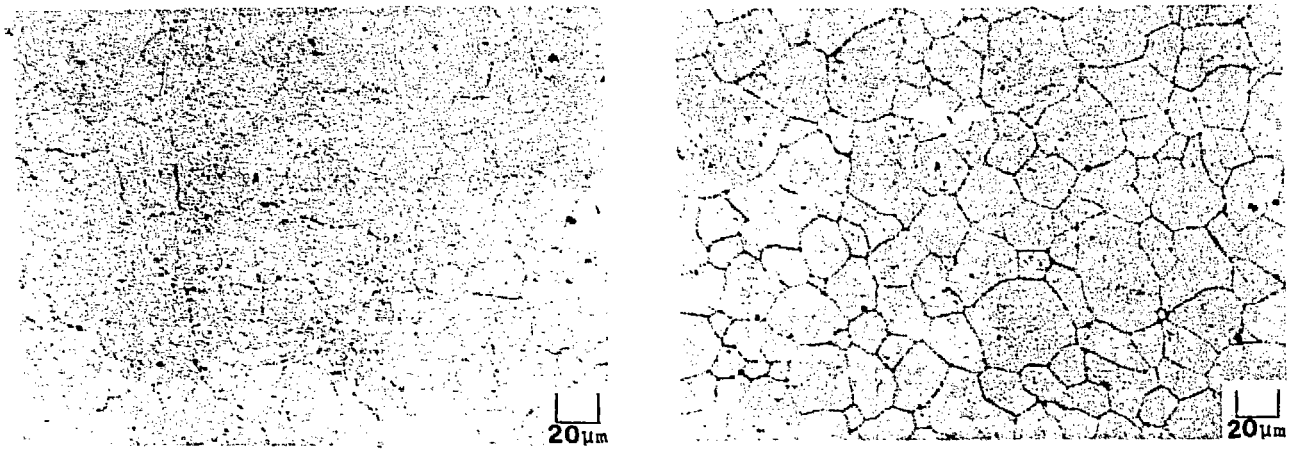

(a) phosphoric acid etch (b) nital etch

Fig. 1. Microstructure of mill-annealed(MA) Alloy 600 tubing

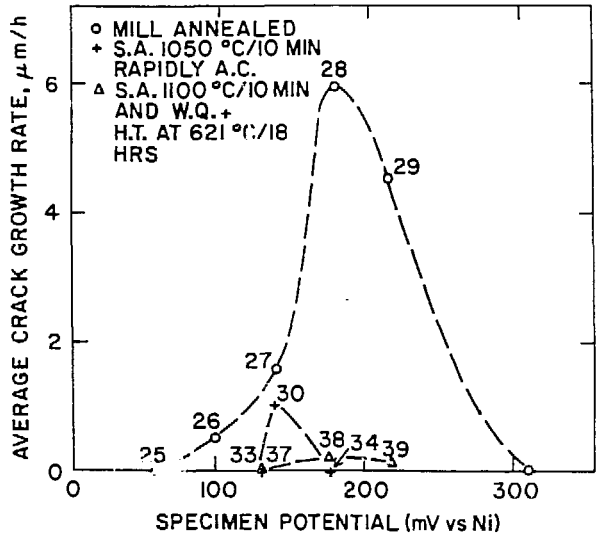

Fig. 2. Relationship between electrochemical potential and average crack propagation rate of C-rings under three different metallurgical conditions in 10% NaOH + 0.1% Na_2CO_3 solution at 300°C. Numbers on figure refer to specimen nos.; test duration 168 hours.

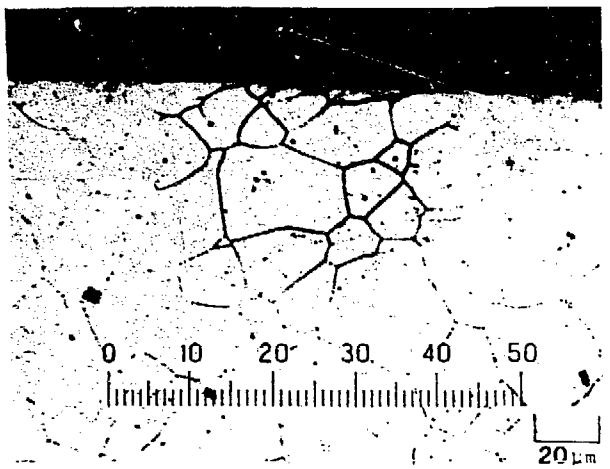

a

b

Fig. 3. Micrographs comparing the phenomena of (a) IGA and (b) SCC produced on MA C-rings in 10% NaOH + 0.1% Na_2CO_3 solution at 300°C.

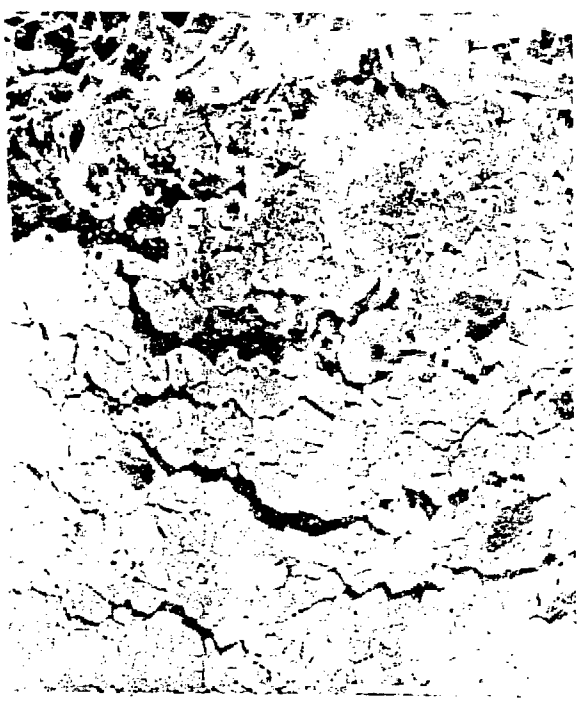

a

b

Fig. 4. SEM micrographs of (a) the cracks initiated and (b) the oxide grooving observed on the sides of the fracture surface of a 0.51mm Alloy 600 wire under constant load (221 MPa nominal) in 10% NaOH + 0.1% Na_2CO_3 solution.

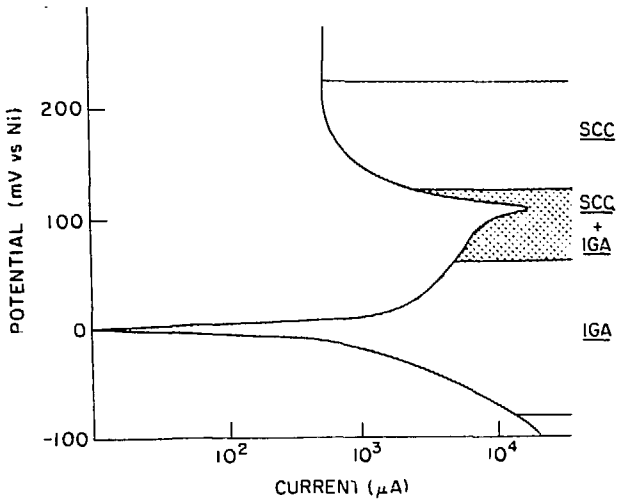

Fig. 5. Superimposition of the potential areas for IGA and SCC on the polarization curve in 10% NaOH + 1% Na_2CO_3 solution at 300°C at a scan rate of 20 mV/min. Specimen area 1 cm^2.

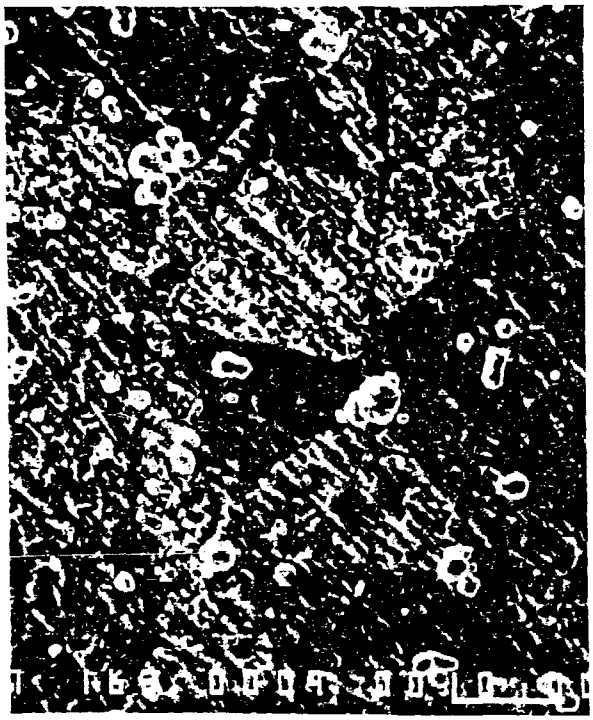

(a) -40 to -50 mV; outside the crevice

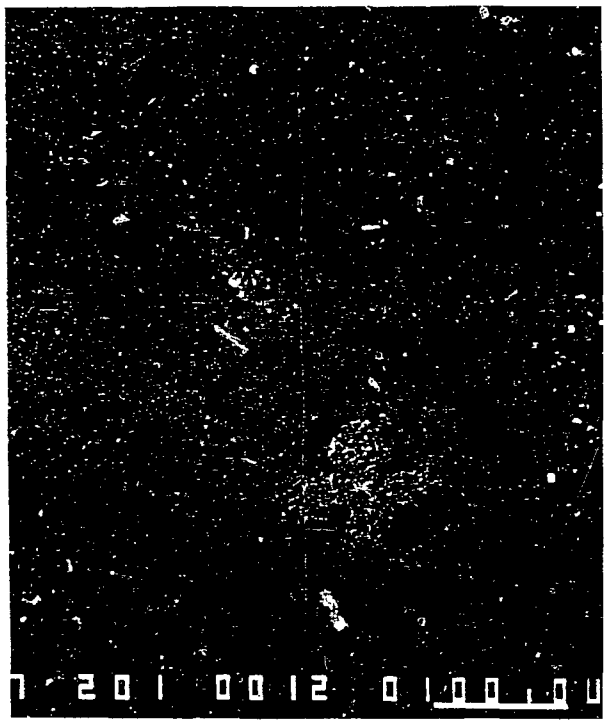

(b) same as (a); inside the crevice

Fig. 6 Continues

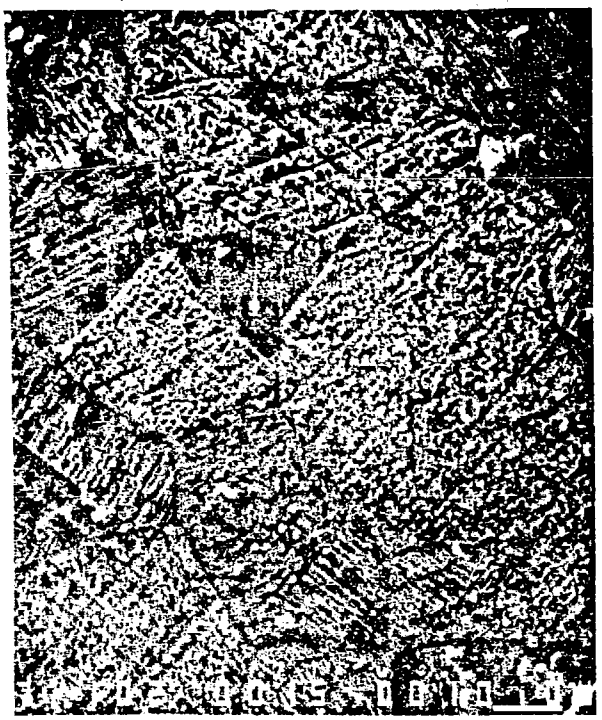

(c) 0 mV; outside the crevice

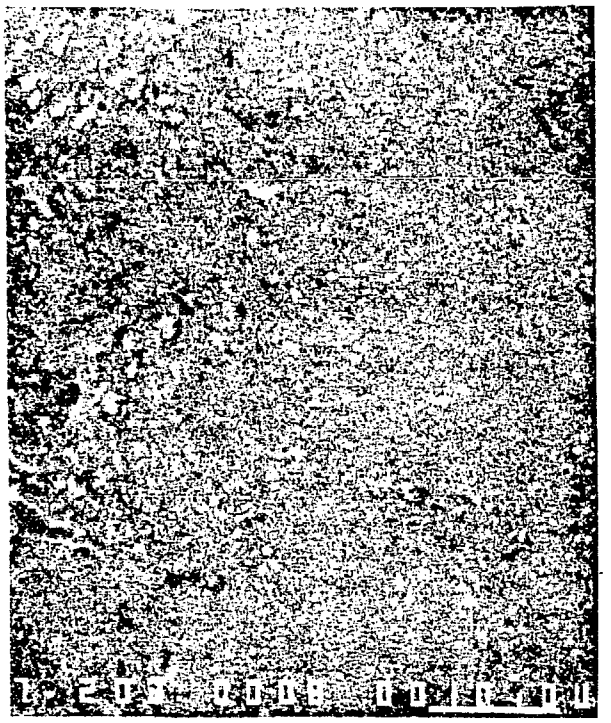

(d) same as (c); inside the crevice

(e) 25 to 45 mV; outside the crevice

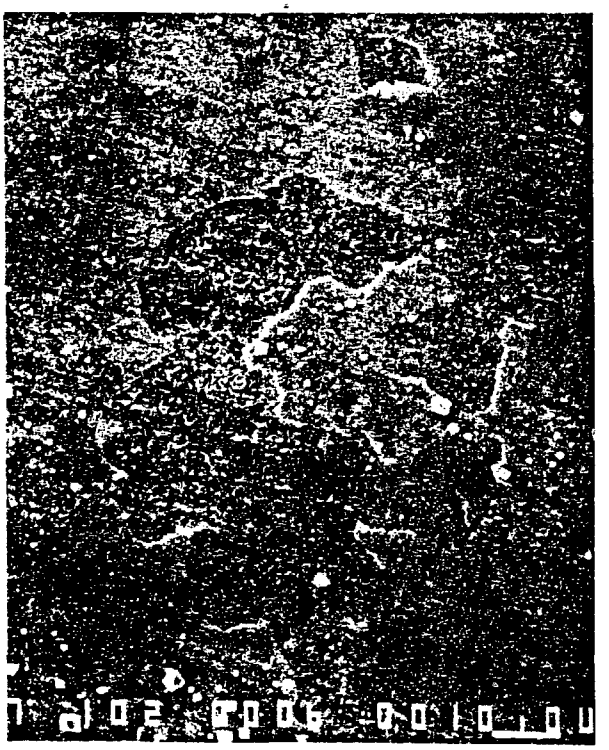

(f) same as (e); inside the crevice

Fig. 6 Continues

(g) 150 mV; outside the crevice

(h) same as (g); outside the crevice showing grain boundary grooving

(i) same as (g); inside the crevice

(j) same as (g); inside the crevice

Fig. 6. Nature of surface attack on Alloy 600 creviced coupons after exposure for 10 days in 10% NaOH + 1% Na_2SO_4 solution at various potentials.